HHS Public Access

Author manuscript

Mech Dev. Author manuscript; available in PMC 2021 September 01.

Published in final edited form as:

Mech Dev. 2020 September ; 163: 103616. doi:10.1016/j.mod.2020.103616.

Mdm4 controls ureteric bud branching via regulation of p53 activity

Sylvia A. Hilliard, **Yuwen Li**, **Angelina Dixon**, **Samir S. El-Dahr**

Tulane University School of Medicine, Department of Pediatrics, Section of Pediatric Nephrology, New Orleans, LA 70112

Abstract

The antagonism between Mdm2 and its close homolog Mdm4 (also known as MdmX) and p53 is vital for embryogenesis and organogenesis. Previously, we demonstrated that targeted disruption of *Mdm2* in the Hoxb7+ ureteric bud (Ub) lineage, which gives rise to the renal collecting system, causes renal hypodysplasia culminating in perinatal lethality. In this study, we examine the unique role of Mdm4 in establishing the collecting duct system of the murine kidney. Hoxb7Cre driven loss of *Mdm4* in the Ub lineage ($Ub^{Mdm4-/-}$) disrupts branching morphogenesis and triggers UB cell apoptosis. $Ub^{Mdm4-/-}$ kidneys exhibit abnormally dilated Ub tips while the medulla is hypoplastic. These structural alterations result in secondary depletion of nephron progenitors and nascent nephrons. As a result, newborn $Ub^{Mdm4-/-}$ mice have hypo-dysplastic kidneys. Transcriptional profiling revealed downregulation of the Ret-tyrosine kinase pathway components, *Gdnf, Wnt11, Sox8, Etv4* and *Cxcr4* in the $Ub^{Mdm4-/-}$ mice relative to controls. Moreover, the expression levels of the canonical Wnt signaling members *Axin2* and *Wnt9b* are downregulated. *Mdm4* deletion upregulated p53 activity and p53-target gene expression including *Cdkn1a* (p21), *Gdf15*, *Ccng1*, *PERP*, and *Fas*. Germline loss of *p53* in $Ub^{Mdm4-/-}$ mice largely rescues kidney development and terminal differentiation of the collecting duct. We conclude that Mdm4 plays a unique and vital role in Ub branching morphogenesis and collecting system development.

Introduction

The Murine double minute (Mdm) RING domain proteins, Mdm2 and Mdm4 (also known as MdmX), are endogenous antagonists of the tumor suppressor protein p53 modulating its stability and activity throughout embryogenesis while maintaining homeostasis of adult tissues (Moyer et al., 2017)). Germline elimination of *Mdm2* or *Mdm4* in mice is embryonic

Corresponding author: Samir S. El-Dahr, MD, Tulane University School of Medicine, Department of Pediatrics, 1430 Tulane Avenue, New Orleans, LA 70112, Tel: (504) 988-6692, Fax: (504) 988-1771, seldahr@tulane.edu.

Author contributions

S. Hilliard: writing original draft, methodology, investigation, data collection, formal analysis, visualization; Y. Li: analysis of microarray data; A. Dixon: methodology, investigation, data collection; S. El-Dahr: Conceptualization, formal analysis, writing – Review and editing, Resources, Supervision, project administration, funding acquisition.

Declaration of competing interest

The authors have no competing or financial interests.

lethal as a result of widespread apoptosis and cell growth arrest (Chavez-Reyes et al., 2003; Jones et al., 1995; Migliorini et al., 2002; Montes de Oca Luna et al., 1995; Parant et al., 2001). However, the co-deletion of *Trp53* in these germline mutants renders them viable allowing embryogenesis to proceed normally (Migliorini et al., 2002; Parant et al., 2001).

In most tissues Mdm2 and Mdm4 function synergistically to efficiently regulate p53 activity (Tanimura et al., 1999; Wu et al., 1993). Mdm2 acts to ensure the rapid proteosomal turnover of p53 while also restricting its transcriptional activity either by directly binding to p53 or triggering its nuclear export. On the other hand, Mdm4 being deficient in E3 ligase function restricts p53 activity by directly engaging its transactivation domain. Mdm4 however enhances Mdm2 protein's E3 ubiquitin ligase activity by dimerizing with it. Disabling the E3 ligase function of Mdm2 does not affect the viability of the mouse mutants since it can adequately inhibit p53 transcriptional activity (Tollini et al., 2014). However, the effects of unbridled p53 activity have lethal consequences in mutant mice where Mdm2 is deficient in both E3 ligase function and its ability to dimerize with Mdm4 (Itahana et al., 2007). Similarly, various Mdm4 RING domain mutants that prevent its interaction with Mdm2 also trigger embryonic lethality (Huang et al., 2011). Thus, the two must act coordinately to keep p53 levels and activity in check during early development.

The definitive kidney in mammals, forms from the intermediate mesoderm (IM). A region of specialized mesenchyme called the metanephric mesenchyme (MM) becomes specified within the caudal IM. Signals from the MM induce the formation of the ureteric bud (Ub), an epithelial evagination of the nephric duct (an epithelial chord within the IM extending along the rostral-caudal axis of the embryo) that ultimately invades the MM. Reciprocal signaling between the two tissue lineages supports repeated branching of the Ub to establish the renal collecting duct system and the ureter (Costantini, 2012; Costantini and Kopan, 2010; Little et al., 2010; Little and McMahon, 2012). Simultaneously, in response to signals from the Ub a subset of the MM becomes resolved into the cap mesenchyme, the precursor of all nephrons, and the stroma from which derive smooth muscle cells, mesangial cells and juxtaglomerular renin cells. Renal hypoplasia with or without accompanying dysplasia is encountered when Ub branching morphogenesis is perturbed. This congenital defect predisposes toward hypertension and often culminates in varying degrees of renal failure in both children and adults (Luyckx et al., 2013).

Previous studies in our laboratory established a requirement for Mdm2 in the morphogenesis of the murine metanephric kidney (Hilliard et al., 2011; Hilliard et al., 2014). We found that Mdm2 mediated suppression of p53 is necessary for the formation of renal epithelial tubules of the kidney. Accordingly, the conditional loss of Mdm2 from the ureteric lineage or the cap mesenchyme stabilizes p53 leading to widespread apoptosis and cell cycle arrest leading to impaired development of the respective tissue lineages. In the absence of Mdm2, the ureteric branches showed lower expression of *Wnt9b*, *Lhx1* and *Pax2* while the cap mesenchyme cells showed reduced expression of *Cited1, Sall1* and *Bmp7*. The co-deletion of p53 rescued Mdm2-triggered renal hypoplasia stemming from p53 stabilization in both tissue compartments affirming the role of p53 in these phenotypic outcomes (Hilliard et al., 2011; Hilliard et al., 2014).

The current study was undertaken to examine unique roles of Mdm4 in establishing the collecting duct system of the kidney. We found that Mdm4 has a non-redundant role in supporting Ub branching morphogenesis. Furthermore, a genome-wide analysis of gene expression changes following Ub-specific loss of Mdm4 revealed disruption of key signaling pathways in branching morphogenesis. The most prominently affected pathways in the $Ub^{Mdm4-/-}$ mutants were the GDNF-Ret receptor tyrosine kinase and Wnt-β-catenin. In addition, we found evidence of elevated expression of p53 target genes which included several of its pro-apoptotic mediators. Most (with the exception of a few persisting cysts) of the $Ub^{Mdm4-/-}$ kidney phenotypes were mitigated in a p53 null background. Thus, the regulation of p53 activity by Mdm4 is required for Ub branching morphogenesis to proceed normally.

Results

$Ub^{Mdm4-/-}$ mice have renal hypoplasia despite the presence of functional Mdm2

RNA analysis by quantitative RT-PCR revealed that Mdm4 gene expression is high in embryonic kidneys and declines postnatally (Fig. 1A). Attempts to examine the spatial expression of Mdm4 protein immunohistochemically were not successful due to lack of suitable antibodies. To examine the role of Mdm4 in Ub branching, we crossed mice with conditional alleles of *Mdm4* (*Mdm4*$^{f/f}$) with *Hoxb7Cre-eGFP* driver mice (Fig. 1B). The progeny developed to term and were recovered at expected Mendelian ratios. Upon gross and histological examination of newborn kidneys, we found that the $Ub^{Mdm4-/-}$ kidneys were smaller in size (Fig. 1 C–F) and exhibited hypoplasia of the nephrogenic zone (defined as the outermost zone of the kidney cortex containing nascent Ub tips and nephrons but excluding maturing glomeruli or proximal tubules) (Fig. 1 G,H) and the renal medulla (Fig. 1 I,J).

Mdm4 function is required for normal ureteric bud branching morphogenesis

To better characterize the hypoplastic phenotype, we followed the branching potential of $Ub^{Mdm4-/-}$ kidneys *ex vivo*. At E12.5, the Ub had branched twice in both $Ub^{Mdm4+/+}$ and $Ub^{Mdm4-/-}$ kidneys (Fig. 2A). We cultured E12.5 $Ub^{Mdm4+/+}$ and $Ub^{Mdm4-/-}$ kidney explants for 72 hours. At the end of culture, the kidneys were fixed and stained for pan cytokeratin (Ub-specific marker) and WT1 (cap mesenchyme and glomerular podocyte marker). The $Ub^{Mdm4-/-}$ kidneys had an obvious reduction in Ub branching by 24 hrs (Fig. 2A) and cytokeratin/$WT1^{+}$ structures at 72 hrs compared to $Ub^{Mdm4+/+}$ control kidneys (Fig. 2 B, C). Quantitation of Ub tips in E12.5 kidney explants at the end of 72 hr culture revealed a 57% (2.3-fold) reduction in $Ub^{Mdm4-/-}$ kidneys (number of Ub tips: 24 ± 4.6, n=3) compared to the wild type controls (56 ± 2.2, n=3) (Fig. 2D). Examination of GFP fluorescence from E13.5 to P0 revealed attenuation of branching morphogenesis in $Ub^{Mdm4-/-}$ as compared to $Ub^{Mdm4+/-}$ kidneys as early as E13.5 *in vivo* (Fig. 2 E). Thus, the Ub of mutant kidneys was able to undergo branching past the T-stage but showed deficits in branching as subsequent development progressed.

Cell proliferation and survival are important determinants of branching morphogenesis (Dziarmaga et al., 2003; Maretto et al., 2003; Michael and Davies, 2004). Therefore, we

examined the cellular basis for the impaired branching morphogenesis seen in the Ub$^{Mdm4-/-}$ mutants. Examination of apoptosis levels using cleaved Caspase 3 immunostaining revealed significant cell death in the Ub lineage (cytokeratin-positive) of the E13.5 mutant kidneys (7.8-fold elevation, p=0.0009) relative to wild type littermate control kidneys (Fig. 3 A–E). Some cells positive for active caspase 3 showed a luminal distribution similar to Ub$^{Mdm2-/-}$ mutant kidneys (Hilliard et al., 2011) (Fig. 3D). Co-immunostaining for phosphorylated histone H3-positive G2/M phase cells and pan cytokeratin at E13.5 did not show a significant change in UB cell proliferation (Fig. 3 F–J). Thus, the elevation in apoptosis contributes to impaired Ub branching morphogenesis seen in the mutants.

Mdm4 loss in the ureteric lineage causes secondary nephrogenesis defects

Since nephron induction depends on reciprocal interactions between the metanephric mesenchyme and Ub compartments, we assessed the effects on Ub-specific deletion of *Mdm4* on nephrogenesis. Deficits in Ub branching yielded fewer nascent nephrons (Lef1/Jagged1-positive) in Ub$^{Mdm4-/-}$ mutants at E14.5-E15.5 (Fig. 4 A–F). Nascent nephron counts were 40% lower in Ub$^{Mdm4-/-}$ than Ub$^{Mdm4+/+}$ kidneys (Fig. 4 E). At this time, when Ub branching is superseded by elongation processes essential for establishing the renal collecting duct system we begin to see cyst-like dilation of the ureteric tips (Fig. 4 F, I, J). The cystic tubules were derived from the ureteric bud lineage (Cytokeratin/E-cadherin positive) (Fig. 4 J, M).

Genome-wide profiling of Ub$^{Mdm4-/-}$ kidneys

In order to determine the differences in gene expression between Ub$^{Mdm4+/+}$ and Ub$^{Mdm4-/-}$ kidneys, we performed a global analysis of gene expression on E14.5 whole kidneys using mouse 4X 44K array from Agilent Technologies. We chose E14.5 for our analyses because of the timing of the onset of the phenotype. A two-color dye-swap strategy was used to compare four wild type and four mutant pools (100ng of total RNA per sample) to minimize bias from signal detection with the Cy3 and Cy5 color channels. Of the 2547 significantly altered genes in our array ($p \leq 0.05$), 1627 were upregulated (range +1.2 to +18.3) while 920 were downregulated (range −1.2 to −4.3) (Fig. 5A). Ingenuity Pathway Analysis-aided analysis of our microarray dataset revealed that the biological functions predicted to be impacted could be resolved into the following categories: (1) disease and disorders 48%; (2) organismal injury and abnormality 23%; (3) metabolism and molecular functions 8%; (4) cellular functions 5% and (5) inflammation 5% (Fig. 5 B). Among the highly up-regulated genes are those encoding the translation initiation factor Eif2s3y, RNA helicase Ddx3y, the cell cycle inhibitor p21 (*Cdkn1a*), the histone H3K4 demethylase Kdm5d, and Growth and differentiation factor 15 (GDF15) (Fig. 5 C). Interestingly, all of these upregulated genes are known p53-target genes. On the other hand, among the highly downregulated genes are immune and RNA binding proteins, the relevance of which to kidney development is unknown (Fig. 5 C).

Loss of Mdm4 impacts Ub tip and stalk networks.

Ret signaling.—Given that branching morphogenesis is disrupted in Ub$^{Mdm4-/-}$ kidneys, we looked for Ub tip and stalk genes showing a differential expression by comparing our

dataset with those published by Rutledge et al (Rutledge et al., 2017). We found 40 genes enriched in the Ub tip that were common to both datasets (Figure 5 D). Of note were *Gfra1* (GDNF/Ret co-receptor), *Sox8*, *Etv4*, *Wnt11*, and *Slco4c1* (organic anion transporter) downstream of Ret signaling with established roles in Ub branching morphogenesis, that were significantly downregulated in $Ub^{Mdm4-/-}$ kidneys. Validation of the microarray results using a few select genes is shown in Fig. 5 E. Moreover, we performed section in situ hybridization of a subset of Ub genes. At E14.5, we found that *Wnt9b* and *Etv4* were downregulated, whereas *c-Ret* and *Emx2* expression remained unchanged (Fig. 6 A–D). At E17.5, c-Ret, Sox8, Wnt11 and Axin2 were downregulated in the Ub tips, while Etv4 remained unchanged (Fig. 6 E–I). Quantitation of Ub tips revealed a significant reduction in Ub tip number at E13.5, E16.5 and E17.5 (Fig. 6 J). We recently identified the transcription factor, p63, a member of the p53 gene family, as a UB tip specific marker expressed transiently during kidney development (El-Dahr et al., 2017). We compared the expression of p63 in $Ub^{Mdm4+/+}$ and $Ub^{Mdm4-/-}$ neonatal kidneys. The expression of p63 was lost in the majority of mutant Ub tips as compared to control kidneys (Fig. 7).

Wnt9b is a paracrine signaling molecule expressed within the Ub stalk. It signals via the β-catenin pathway to promote renewal of the progenitor cap mesenchyme cells (dorsally) and induce differentiation of the PTA (ventrally) (Karner et al., 2011). Since our microarray and qPCR data showed lower levels of *Wnt9b* transcripts, we compared our dataset with that of Karner *et al* (Karner et al., 2011) to see if cognate Wnt9b targets within the metanephric mesenchyme are downregulated in our dataset (Table 1). We find that some of the genes downregulated in $Wnt9b^{-/-}$ kidneys and with bona-fide Lef/Tcf binding sites were similarly downregulated in our dataset. These include nephron inducing genes *Wnt4, Cdh4*, *Pax8*, *Cxcr4*, and *Lef1*. Simultaneously, the expression of a few Wnt9b targets which support renewal of the progenitor cap mesenchyme such as *Gpx6* and *Itga8* were upregulated in our dataset. Furthermore, upregulation and downregulation of some of the genes were reminiscent of those reported in $Ctnnb1^{-/-}$ kidneys (Suppl. Tables 1, 2). Therefore, deficiency of Mdm4 targeted to Ub cells alters the transcript levels of key tip and stalk genes critical for branching morphogenesis and nephron specification. Lastly, we performed HALLMARK pathway analysis to determine the enrichment of select gene set pathways associated with the $Ub^{Mdm4-/-}$ phenotype and found that the top enriched pathways included Epithelial-mesenchymal transition, p53, apoptosis, Wnt-b-catenin, and Notch among others (Suppl. Fig. S-1).

Ub-specific deletion of Mdm4 activates p53-dependent pathways.

Given that Mdm4 can regulate p53 transactivation function, we looked for transcript level changes in p53 target genes in the whole-mouse genome following Mdm4 deletion from the Ub. Previously, the widely recognized role of p53 as a tumor suppressor largely overshadowed its contribution to development, differentiation, metabolism, autophagy, aging etc. (Kastenhuber and Lowe, 2017). The nuanced nature of developmental phenotypes encountered in $p53^{-/-}$ mice became evident later on against different mouse strain backgrounds and includes reduced survival, exencephaly, craniofacial abnormalities, congenital anomalies of the kidney and urinary tract, lung defects, and/or reduced fertility of female mice (Armstrong et al., 1995; Donehower et al., 1992; Hu et al., 2007; Kaufman et

al., 1997; Rinon et al., 2011; Saifudeen et al., 2009; Tateossian et al., 2015). The corollary, where p53 levels and activity are above what is physiologically normal, similarly poses developmental challenges in multiple tissues and organs including the kidney (Hilliard et al., 2011; Hilliard et al., 2014; Moyer et al., 2017). We found that the abrogation of Mdm4 function from the ureteric epithelia increases p53 transactivation. The most significant changes observed were in p53 target genes modulating the cell cycle (*Cdkn1a*, *Ccng1*), cellular apoptosis (*Fas*, *Apaf1*, *Perp*, *p53INP1*), EMT and invasion (*snai2* or SLUG, *Pai1* or serpine 2), or inflammation (*Thbs1*, *Adgrb1*) (Table 2). Absence of Mdm4 in the Ub affects cell survival and cell fate and ultimately branching morphogenesis.

In order to delineate the p53-mediated gene changes specific to the kidney, we compared our dataset to that derived from our previously published p53-Chip sequencing of E15.5 kidneys (Li et al., 2013). We found 464 gene targets shared by the two datasets (Table 3). Of them, the genes pertinent to Ub morphogenesis and differentiation and bound by p53 are *Wnt11, Axin2, Ctnnb1, Gja1, Tcf4, Lgr4 Etv4, Ptch1, Calb1, Crlf1* and *Pde5a*.

Elimination of p53 function rescues Ub$^{Mdm4-/-}$ kidney phenotype

Given the strong involvement of p53 regulated genes in the Ub$^{Mdm4-/-}$ kidney phenotype, we bred Ub$^{Mdm4-/-}$ mice into a p53 null background. We found that the Ub$^{Mdm4-/-}$; *Trp53*$^{+/+}$ mice have small kidneys (Fig. 8 A, B, D, E). However, the size and histology of Ub$^{Mdm4-/-}$; *Trp53*$^{-/-}$ kidneys resembles those of control kidneys (Fig. 8 A, C, D, F). The Ub$^{Mdm4+/-}$; *p53*$^{+/+}$ kidneys show a 15% reduction while the Ub$^{Mdm4-/-}$ *p53*$^{+/+}$ kidneys show a 41% reduction in surface area when compared to control kidneys (Fig. 8 G). The loss of a single allele of *Trp53* (Ub$^{Mdm4-/-}$ *p53*$^{+/-}$) brings about a partial rescue (27% reduction in kidney area) while loss of both *Trp53* alleles narrows it further to 8% reduction in kidney area relative to control kidneys (Fig. 8 G). Comparison of neonatal Ub$^{Mdm4+/+}$; *p53*$^{+/+}$, Ub$^{Mdm4-/-}$; *p53*$^{+/+}$; and Ub $^{Mdm4-/-}$; *p53*$^{-/-}$ kidneys by co-immunostaining for Six2 and pan cytokeratin confirms restoration of gross morphology and histological patterning of the medulla and nephron progenitors (Fig. 8 H–J).

To confirm if Wnt-β-catenin signaling downstream of p53 regulation is restored in the kidneys of rescued mice, we performed in situ hybridization for *Axin2* a target of canonical Wnt signaling. In the absence of functional *p53*, the levels of *Axin2* are restored in the Ub$^{Mdm4-/-}$; *p53*$^{-/-}$ medulla compared to Ub$^{Mdm4-/-}$; *p53*$^{+/+}$ kidneys (Fig. 9 A–F). Similarly, in newborn mice the expression of the Wnt-β-catenin nuclear effector Lef1 shows severe downregulation in the Ub and associated nascent nephrons in Ub$^{Mdm4-/-}$ kidneys but is restored to wild type levels in the *p53* null rescued kidneys (Fig. 9 G–I). This is illustrated schematically in Fig. 9 J–L.

The extent of rescue on a p53 null background was evident in histological analysis of P20 kidneys from Ub$^{Mdm4+/+}$; *p53*$^{+/+}$, Ub$^{Mdm4-/-}$; *p53*$^{+/+}$; and Ub $^{Mdm4-/-}$; *p53*$^{-/-}$ mice. The Ub$^{Mdm4-/-}$ kidneys are severely dysmorphic in gross appearance and have prominent deficits in medullary collecting ducts formation resulting in severe hydronephrosis (Suppl. Fig. S-2). The histology of Ub$^{Mdm4-/-}$ kidneys in a p53 null background shows restoration of kidney architecture including the outer medulla (Suppl. Fig. S-2).

Discussion

The regulation of p53 is carefully orchestrated during embryonic development, differentiation, and aging (Tyner et al., 2002; Van Nostrand et al., 2017; Van Nostrand et al., 2014). This is exemplified by the p53-dependent embryonic lethal phenotype following the loss of either gene, Mdm2 or Mdm4 (Jones et al., 1995; Montes de Oca Luna et al., 1995; Parant et al., 2001). The p53 antagonists, Mdm2 and Mdm4, despite their homology and similar modular domains function non-redundantly. Notably, Mdm4 regulation of p53 appears to vary with cellular context (Barboza et al., 2008; Maetens et al., 2007; Mancini and Moretti, 2009). Therefore, loss of Mdm4 triggers cell apoptosis in neuronal and intestinal cells but not in cardiomyocytes, erythroid, and smooth muscle cells where the overwhelming response is cell cycle arrest or impaired cellular proliferation (Boesten et al., 2006; Grier et al., 2006; Maetens et al., 2007; Migliorini et al., 2002; Valentin-Vega et al., 2009). Furthermore, the development and morphogenesis of certain organs like the CNS, eye lens, and endocrine component of pancreas require synergistic interactions between Mdm2 and Mdm4 (Francoz et al., 2006; Xiong et al., 2006; Zhang et al., 2017; Zhang et al., 2014).

The aim of this study was threefold. First, we wanted to determine if Mdm4 has a role in supporting Ub branching morphogenesis. Secondly, with the aid of genome-wide transcript analyses of whole mouse kidneys we looked for p53 dependent and independent alterations in gene expression following *Mdm4* loss from ureteric epithelia. Lastly, we examined the contribution of p53 to the mutant phenotype by one or two allele loss of p53. We found that the similar to Mdm2 (Hilliard et al., 2014), *Mdm4* expression is high in the developing kidney and declines during postnatal maturation. The $Ub^{Mdm4-/-}$ kidneys are small and hypoplastic with reduced Ub branching morphogenesis. The downregulation of GDNF-Ret and Wnt/β-catenin signaling together with elevation of p53 transactivation function appear to be contributing to the $Ub^{Mdm4-/-}$ mutant phenotypes. Therefore, like Mdm2, Mdm4 has an independent role in modulating Ub branching. This study did not address whether Mdm2 compensates for lack of Mdm4 as this requires generation and investigation of double *Mdm2/Mdm4* mutants.

Changes in the physiological levels of p53 in response to varying degrees of stress have differing outcomes on cell fate (Vousden, 2002; Vousden and Lane, 2007). Under mild stress p53 induces cell cycle arrest allowing for DNA repair to proceed. Conversely, under acute stress p53 triggers senescence or apoptosis of the affected cells. Even mild elevation of p53 levels as encountered with Mdm2-Mdm4 haplo-insufficiency confers a growth disadvantage on cells (Terzian et al., 2007; Zhang et al., 2017). Of the 200 known p53 targets, 105 show changes in expression in our microarray, consistent with the activation of p53.

Several effectors of the GDNF-Ret-Wnt11 auto-regulatory feedback loop are downregulated in our array. The GDNF-Ret receptor tyrosine kinase pathway has a prominent role in ureteric branching and confers Ub tip identity by inducing Vsnl1, Ret, Sox 8/9, Etv4/5, and Wnt11 expression exclusively in the tip domain (Lu et al., 2009; Ola et al., 2011; Reginensi et al., 2011). The $Ub^{Mdm4-/-}$ kidneys showed downregulation of selective targets _ *Vsnl1*, *Sox8*, *Etv4* and *Wnt11*, of this pathway.

Ub specific loss of Mdm4 results in the attenuated expression of canonical Wnt pathway molecules. Supporting this notion is the diminished expression of Wnt ligands (*Wnt9b, Wnt11*, and *Wnt4*) and effector molecules (*Ctnnb1*, *Tcf4*, and *Lef1*) coupled with upregulation of endogenous inhibitors such as *Dkk2* and *Sfrp4*. Kim et al. (Kim et al., 2011) found that p53 typically represses canonical Wnt targets _ β-catenin, Lef1, Axin2, through the transactivation of miR-34. Thus, the downregulation of Wnt-β catenin signaling is consistent with up regulation of p53 transactivation in our array. In the developing kidney, β-catenin is required to maintain the Ub tip progenitors and loss of its function from the ureteric lineage results in renal agenesis or hypoplasia (Bridgewater et al., 2008; Marose et al., 2008). Thus, downregulation of Wnt signaling would further explain the hypoplastic phenotype encountered upon Mdm4 loss from the Ub lineage.

In conclusion, the repression of p53 function by Mdm4 supports Ub branching morphogenesis and formation of the collecting system. Apart from elevated p53 transactivation, the Ub-specific loss of Mdm4 results in the disruption of major signaling pathways guiding Ub branching. Differential gene analyses revealed suboptimal expression of several of the tip and stalk genes which would explain the aberrant branching phenotype and hypoplastic kidneys. Surprisingly, despite the elevated expression of *Cdkn1a* the overwhelming p53 response in the $Ub^{Mdm4-/-}$ kidneys appears to be pro-apoptotic. Comparison of differentiated cell markers within the collecting ducts of neonatal kidneys showed heightened p53 activity in Mdm4 mutant kidneys which disrupts terminal differentiation. Eliminating p53 in these mutants restores Ub branching morphogenesis and collecting duct development.

Materials and Methods

Animals

Animal protocols utilized in this study were in adherence to the guidelines outlined by the Institutional Animal Care and Use Committee in accordance with NIH. The *Mdm4 floxed* mice (Grier *et al.*, 2006) originally from Dr. G. Lozano, were a gift from Dr. Hua Lu. The *Mdm2 floxed* mice (01XH9, Dr. Mary Ellen Perry) were initially obtained from the NCI repository (Frederick MD) while the *Hoxb7-Egfp-Cre* mice (Zhao et al., 2004) were a kind gift from Dr. Carlton Bates. The $p53^{+/-}$ mice (Jacks et al., 1994) obtained from The Jackson Laboratory (Bar Harbor, Maine, USA) were used in our rescue experiments. The specifications for genotyping were outlined by the respective vendors for *Mdm2-floxed* mice and *p53* conventional mutant mice. To distinguish between *Mdm4* wild-type and conditional alleles the following primer set was used (Grier et al., 2006):

F3, 5’-GGTGTCCTTGAACTTGCTGTGTAGAA-3’,

E2re, 5’-CTGGGCCGAGGTGGAATGTGATGT-3’

The *Cre* transgene was genotyped using the following primer pair:

Forward primer: 5’ -ACCAGCCAGCTATCAACTC-3’

Reverse primer: 5’ -TATACGCGTGCTAGCGAAGATCTCCATCTTCCAGCAG-3’

The breeding strategy used involved crossing *Hoxb7-Egfp-Cre* $^{tg/-}$*; Mdm4* $^{flox/+}$ male mice to *Mdm4* $^{flox/flox}$ (Mdm4$^{fl/fl}$) female mice. The *p53* rescue experiments involved crossing *Hoxb7-Egfp-Cre*$^{tg/-}$*; Mdm4 flox*/+; *p53*$^{+/-}$ males to *Mdm4 flox/flox; p53*$^{+/-}$ females. For all timed pregnancies, noon of the day on which the vaginal plug was detected was regarded as embryonic day (E) 0.5.

Gross Morphology

All bright field images were captured using the Nikon SMZ100 stereo microscope mounted with a DS-Fi1 camera. The images were processed using NIS Elements software (Nikon, NY, USA).

Histology

Freshly isolated kidneys were rinsed in ice-cold PBS and fixed overnight in 10% buffered formalin (for histology or IF) or 4% PFA/PBS (for section ISH) at 4C. Following serial alcohol dehydration and clearing in Xylene, the samples were embedded in paraffin. Paraffin embedded kidneys were sectioned either at 4 um (for immunofluorescence staining) or 10um (for in situ hybridization detection).

Hematoxylin and Eosin Staining

Routine Hematoxylin and Eosin staining (Richard-Allan Scientific, ThermoFisher Scientific) was performed on age matched wildtype control and mutant kidney sections (4um). The protocol used was the one outlined by the manufacturer. Slides were mounted in Permount (Electron Microscopy Sciences, VWR) mounting media. Images were captured using a Nikon Digital-Sight DS-U3 camera mounted on a Nikon Eclipse Ni Fluorescent Scope. Images were processed using NIS elements (version 4.4) software.

Organ Culture

Ex vivo kidney explants were grown in 6-well tissue culture treated Transwell plates with 24mm membrane inserts (Cat#3450 Corning Inc.) with a pore size of 0.4um. The kidneys were cultured in Advanced DMEM/F-12 medium (Invitrogen) supplemented with 10% fetal calf serum and 1% penicillin streptomycin (10,000 U/ml, ThermoFisher Scientific) at the air-medium interface in 5% CO_2 atmosphere at 37°C. To examine ureteric branching morphogenesis the kidney explants were cultured for up to 72 h. Images were captured using an Olympus BX51 fluorescence microscope.

Immunostaining

Clearing and rehydration of paraffin sections (4um) was followed with antigen retrieval (10mM Sodium Citrate, pH 6.0) in a steamer for 45 min. Endogenous peroxidase was quenched by incubating slides in 3% hydrogen peroxide at room temperature. Sections were blocked for 90 min at room temperature in 0.5% blocking reagent (Perkin-Elmer FP1012) in Tris-buffered saline supplemented with 10% normal donkey serum together with unconjugated, monovalent donkey anti-Rabbit Fab (711-007-003 Jackson Immunoresearch laboratories, Inc., PA) and donkey anti-Mouse Fab (715-007-003) fragments at 15 μl/ml each. Primary antibodies used were goat anti-AQP2 (C17, sc-9882, Santa cruz), anti-rabbit

Calbindin (ab25085, Abcam), rabbit anti cleaved caspase 3 (Asp 175, Cat# 9661, Cell Signaling), mouse pan Cytokeratin (C2562, Sigma), mouse anti-E-cadherin (610181, BD Biosciences), rabbit phospho-histone H3 (Ser 10) antibody (9701,Cell Signaling), rabbit anti-Jagged1 (H114, Cat# sc-8303, Santa Cruz), rabbit anti-LEF1 (C12A5, Cat #2230, Cell Signaling), mouse anti-p63 (SFI-6, DCS Immunoline), rabbit anti-Six2 (11562-1-AP, Proteintech), goat anti-V-ATPase (B1) (N-20, cat# sc-21206), rabbit anti-V-ATPase (B1/B2) (H-180, sc-20943), rabbit anti-WT1 (C-19:sc-192, Santa Cruz), and DAPI (D1306, Invitrogen).

For secondary detection we used donkey anti-rabbit, donkey anti-mouse, or donkey anti goat antibodies as was required, conjugated to one of the following Alexafluor dyes: Alexa-Fluor555, AlexaFluor488 or AlexaFluor 647 (Molecular Probes, Invitrogen). The Tyramide Signal Amplification (TSA) fluorescence kit (NEL760001KT, Perkin Elmer) was used in instances where the secondary antibody was conjugated to horse radish peroxidase enzyme instead of a fluorophore. The immunofluorescent images were captured with a Zyla/Andor camera mounted on a Nikon Eclipse Ni fluorescent microscope. The confocal images were captured with the aid of the Confocal Nikon eclipse Ti2 scope.

Quantitative reverse transcriptase-polymerase chain reaction (qRT-PCR)

Quantitative qRT-PCR was performed on total RNA isolated from E14.5 kidneys using the RNeasy Mini Kit (Qiagen). Real-time primer-probe mixes were ordered from Applied Biosystems. The assay was done using the Taqman RNA-to-CT 1step kit (4392938; Applied Biosystems, New York, U.S.A). The thermal profile used was as follows: 48°C for 15min, 95°C for 10min and 40 cycles of 95°C for 15s, 55°C for 1 min and 72°C for 1 min. The reactions were performed in triplicate. The relative transcript levels were calculated using the ΔΔCt method with GAPDH as the endogenous normalizing gene. Three independent experiments using total RNA from kidneys of representative genotypes from age-matched litters were used in our assays. The scale bars represent the standard error of mean of average values. P value was calculated using the two-tailed Student's T test with a probability of 0.05 considered as significant.

Gene	Primer-Probe
Axin2	Mm00443610_m1
Bax	Mm00432050_m1
Cdkn1a	Mm00432448_m1
Ccng1	Mm00438084_m1
Emx2	Mm00550241_m1
Etv4	Mm00476696_m1
Gapdh VIC_PL	Mm99999915_g1
Gdf15	Mm00442228_m1
Sox8	Mm00803422_m1
Wnt9b	Mm01248219_m1

Gene	Primer-Probe
Wnt11	Mm00437328_m1

In situ Hybridization

In situ hybridization protocol used has been previously described (Hilliard et al., 2011). The samples were fixed overnight in 4%PFA/PBS and prepared for paraffin embedding. The samples were sectioned at 10um. Digoxigenin labeled RNA probes were used to bind the endogenous transcripts in situ. Probe binding was detected using anti-Digoxigenin Fab fragments coupled to Alkaline Phosphatase (Roche Diagnostics) and the chromogenic substrate BM purple.

Genome-wide Microarray Analysis

Microarray analysis was performed using Agilent's 'Two color Microarray Based Gene Expression Analysis (Agilent G4140–90050). The assay used 100ng of total RNA isolated from E14.5 whole mouse kidney explants (four pools of wild type matched with four pools of mutant samples) using the RNeasy Mini Kit (Qiagen). The quality of RNA samples was assessed on a Bio Analyzer (Agilent 2100, Palo Alto, CA). Fluorescently labeled (Cy3-CTP or Cy5-CTP) cRNA was generated from 100 ng of total RNA using the Low input quick amp labeling protocol from Agilent. The labeled cRNA was hybridized to Agilent's 4X 44K whole mouse genome microarray slide. The arrays were scanned using a dual-laser DNA microarray scanner (Agilent). To prevent bias from signal detection with different color dyes (Cy5, Cy3), we applied dye-swap strategy to this experiment, in which identical sample pairs were reverse labeled. The data were then extracted by the Feature Extraction 6.1 software (Agilent). Raw data were processed using GeneSpring GX (version 13.0) software. Only genes, showing a significant ($P \leq 0.05$) differential change in expression after Benjamini and Hochberg false discovery rate (FDR) correction in the four datasets, were used for further analyses. Additional analysis of the microarray data was completed using the Ingenuity Pathway Analysis (IPA) software (Qiagen, CA). The raw data is deposited in GEO under GSE137994.

Statistical Analysis.

All experiments were performed on 3–4 biological replicates as indicated in the text. Statistical differences were performed using t-test or one-way ANOVA. A p-value <0.05 was considered statistically significant.

Supplementary Material

Refer to Web version on PubMed Central for supplementary material.

Acknowledgments

We thank Yuwen Li (Hayward Genetics Center, Tulane) for assistance in microarray hybridization analysis and the Tulane Renal & Hypertension Center core facilities. We thank Dr. Carl Bates for Hoxb7-Cre-eGFP mice.

Funding

This work is supported by RO1-DK 62550 from the National Institutes of Health.

References

Armstrong JF, Kaufman MH, Harrison DJ, Clarke AR, 1995 High-frequency developmental abnormalities in p53-deficient mice. Curr Biol 5, 931–936. [PubMed: 7583151]

Barboza JA, Iwakuma T, Terzian T, El-Naggar AK, Lozano G, 2008 Mdm2 and Mdm4 loss regulates distinct p53 activities. Mol Cancer Res 6, 947–954. [PubMed: 18567799]

Boesten LS, Zadelaar SM, De Clercq S, Francoz S, van Nieuwkoop A, Biessen EA, Hofmann F, Feil S, Feil R, Jochemsen AG, Zurcher C, Havekes LM, van Vlijmen BJ, Marine JC, 2006 Mdm2, but not Mdm4, protects terminally differentiated smooth muscle cells from p53-mediated caspase-3-independent cell death. Cell Death Differ 13, 2089–2098. [PubMed: 16729027]

Bridgewater D, Cox B, Cain J, Lau A, Athaide V, Gill PS, Kuure S, Sainio K, Rosenblum ND, 2008 Canonical WNT/beta-catenin signaling is required for ureteric branching. Dev Biol 317, 83–94. [PubMed: 18358465]

Chavez-Reyes A, Parant JM, Amelse LL, de Oca Luna RM, Korsmeyer SJ, Lozano G, 2003 Switching mechanisms of cell death in mdm2- and mdm4-null mice by deletion of p53 downstream targets. Cancer Res 63, 8664–8669. [PubMed: 14695178]

Costantini F, 2012 Genetic controls and cellular behaviors in branching morphogenesis of the renal collecting system. Wiley Interdiscip Rev Dev Biol 1, 693–713. [PubMed: 22942910]

Costantini F, Kopan R, 2010 Patterning a complex organ: branching morphogenesis and nephron segmentation in kidney development. Dev Cell 18, 698–712. [PubMed: 20493806]

Donehower LA, Harvey M, Slagle BL, McArthur MJ, Montgomery CA Jr., Butel JS, Bradley A, 1992 Mice deficient for p53 are developmentally normal but susceptible to spontaneous tumours. Nature 356, 215–221. [PubMed: 1552940]

Dziarmaga A, Clark P, Stayner C, Julien JP, Torban E, Goodyer P, Eccles M, 2003 Ureteric bud apoptosis and renal hypoplasia in transgenic PAX2-Bax fetal mice mimics the renal-coloboma syndrome. J Am Soc Nephrol 14, 2767–2774. [PubMed: 14569086]

Francoz S, Froment P, Bogaerts S, De Clercq S, Maetens M, Doumont G, Bellefroid E, Marine JC, 2006 Mdm4 and Mdm2 cooperate to inhibit p53 activity in proliferating and quiescent cells in vivo. Proc Natl Acad Sci U S A 103, 3232–3237. [PubMed: 16492744]

Grier JD, Xiong S, Elizondo-Fraire AC, Parant JM, Lozano G, 2006 Tissue-specific differences of p53 inhibition by Mdm2 and Mdm4. Mol Cell Biol 26, 192–198. [PubMed: 16354690]

Hilliard S, Aboudehen K, Yao X, El-Dahr SS, 2011 Tight regulation of p53 activity by Mdm2 is required for ureteric bud growth and branching. Dev Biol 353, 354–366. [PubMed: 21420949]

Hilliard SA, Yao X, El-Dahr SS, 2014 Mdm2 is required for maintenance of the nephrogenic niche. Dev Biol 387, 1–14. [PubMed: 24440154]

Hu W, Feng Z, Teresky AK, Levine AJ, 2007 p53 regulates maternal reproduction through LIF. Nature 450, 721–724. [PubMed: 18046411]

Huang L, Yan Z, Liao X, Li Y, Yang J, Wang ZG, Zuo Y, Kawai H, Shadfan M, Ganapathy S, Yuan ZM, 2011 The p53 inhibitors MDM2/MDMX complex is required for control of p53 activity in vivo. Proc Natl Acad Sci U S A 108, 12001–12006. [PubMed: 21730163]

Itahana K, Mao H, Jin A, Itahana Y, Clegg HV, Lindstrom MS, Bhat KP, Godfrey VL, Evan GI, Zhang Y, 2007 Targeted inactivation of Mdm2 RING finger E3 ubiquitin ligase activity in the mouse reveals mechanistic insights into p53 regulation. Cancer Cell 12, 355–366. [PubMed: 17936560]

Jacks T, Remington L, Williams BO, Schmitt EM, Halachmi S, Bronson RT, Weinberg RA, 1994 Tumor spectrum analysis in p53-mutant mice. Curr Biol 4, 1–7. [PubMed: 7922305]

Jones SN, Roe AE, Donehower LA, Bradley A, 1995 Rescue of embryonic lethality in Mdm2-deficient mice by absence of p53. Nature 378, 206–208. [PubMed: 7477327]

Karner CM, Das A, Ma Z, Self M, Chen C, Lum L, Oliver G, Carroll TJ, 2011 Canonical Wnt9b signaling balances progenitor cell expansion and differentiation during kidney development. Development 138, 1247–1257. [PubMed: 21350016]

Kastenhuber ER, Lowe SW, 2017 Putting p53 in Context. Cell 170, 1062–1078. [PubMed: 28886379]

Kaufman MH, Kaufman DB, Brune RM, Stark M, Armstrong JF, Clarke AR, 1997 Analysis of fused maxillary incisor dentition in p53-deficient exencephalic mice. J Anat 191 (Pt 1), 57–64. [PubMed: 9279659]

Kim NH, Kim HS, Kim NG, Lee I, Choi HS, Li XY, Kang SE, Cha SY, Ryu JK, Na JM, Park C, Kim K, Lee S, Gumbiner BM, Yook JI, Weiss SJ, 2011 p53 and microRNA-34 are suppressors of canonical Wnt signaling. Sci Signal 4, ra71. [PubMed: 22045851]

Li Y, Liu J, McLaughlin N, Bachvarov D, Saifudeen Z, El-Dahr SS, 2013 Genome-wide analysis of the p53 gene regulatory network in the developing mouse kidney. Physiol Genomics 45, 948–964. [PubMed: 24003036]

Little M, Georgas K, Pennisi D, Wilkinson L, 2010 Kidney development: two tales of tubulogenesis. Curr Top Dev Biol 90, 193–229. [PubMed: 20691850]

Little MH, McMahon AP, 2012 Mammalian kidney development: principles, progress, and projections. Cold Spring Harb Perspect Biol 4.

Lu BC, Cebrian C, Chi X, Kuure S, Kuo R, Bates CM, Arber S, Hassell J, MacNeil L, Hoshi M, Jain S, Asai N, Takahashi M, Schmidt-Ott KM, Barasch J, D'Agati V, Costantini F, 2009 Etv4 and Etv5 are required downstream of GDNF and Ret for kidney branching morphogenesis. Nat Genet 41, 1295–1302. [PubMed: 19898483]

Luyckx VA, Bertram JF, Brenner BM, Fall C, Hoy WE, Ozanne SE, Vikse BE, 2013 Effect of fetal and child health on kidney development and long-term risk of hypertension and kidney disease. Lancet 382, 273–283. [PubMed: 23727166]

Maetens M, Doumont G, Clercq SD, Francoz S, Froment P, Bellefroid E, Klingmuller U, Lozano G, Marine JC, 2007 Distinct roles of Mdm2 and Mdm4 in red cell production. Blood 109, 2630–2633. [PubMed: 17105817]

Mancini F, Moretti F, 2009 Mitochondrial MDM4 (MDMX): an unpredicted role in the p53-mediated intrinsic apoptotic pathway. Cell Cycle 8, 3854–3859. [PubMed: 19887911]

Maretto S, Cordenonsi M, Dupont S, Braghetta P, Broccoli V, Hassan AB, Volpin D, Bressan GM, Piccolo S, 2003 Mapping Wnt/beta-catenin signaling during mouse development and in colorectal tumors. Proc Natl Acad Sci U S A 100, 3299–3304. [PubMed: 12626757]

Marose TD, Merkel CE, McMahon AP, Carroll TJ, 2008 Beta-catenin is necessary to keep cells of ureteric bud/Wolffian duct epithelium in a precursor state. Dev Biol 314, 112–126. [PubMed: 18177851]

Michael L, Davies JA, 2004 Pattern and regulation of cell proliferation during murine ureteric bud development. J Anat 204, 241–255. [PubMed: 15061751]

Migliorini D, Lazzerini Denchi E, Danovi D, Jochemsen A, Capillo M, Gobbi A, Helin K, Pelicci PG, Marine JC, 2002 Mdm4 (Mdmx) regulates p53-induced growth arrest and neuronal cell death during early embryonic mouse development. Mol Cell Biol 22, 5527–5538. [PubMed: 12101245]

Montes de Oca Luna R, Wagner DS, Lozano G, 1995 Rescue of early embryonic lethality in mdm2-deficient mice by deletion of p53. Nature 378, 203–206. [PubMed: 7477326]

Moyer SM, Larsson CA, Lozano G, 2017 Mdm proteins: critical regulators of embry ogenesis and homeostasis. J Mol Cell Biol.

Ola R, Jakobson M, Kvist J, Perala N, Kuure S, Braunewell KH, Bridgewater D, Rosenblum ND, Chilov D, Immonen T, Sainio K, Sariola H, 2011 The GDNF target Vsnl1 marks the ureteric tip. J Am Soc Nephrol 22, 274–284. [PubMed: 21289216]

Parant JM, Reinke V, Mims B, Lozano G, 2001 Organization, expression, and localization of the murine mdmx gene and pseudogene. Gene 270, 277–283. [PubMed: 11404026]

Reginensi A, Clarkson M, Neirijnck Y, Lu B, Ohyama T, Groves AK, Sock E, Wegner M, Costantini F, Chaboissier MC, Schedl A, 2011 SOX9 controls epithelial branching by activating RET effector genes during kidney development. Hum Mol Genet 20, 1143–1153. [PubMed: 21212101]

Rinon A, Molchadsky A, Nathan E, Yovel G, Rotter V, Sarig R, Tzahor E, 2011 p53 coordinates cranial neural crest cell growth and epithelial-mesenchymal transition/delamination processes. Development 138, 1827–1838. [PubMed: 21447558]

Rutledge EA, Benazet JD, McMahon AP, 2017 Cellular heterogeneity in the ureteric progenitor niche and distinct profiles of branching morphogenesis in organ development. Development 144, 3177–3188. [PubMed: 28705898]

Saifudeen Z, Dipp S, Stefkova J, Yao X, Lookabaugh S, El-Dahr SS, 2009 p53 regulates metanephric development. J Am Soc Nephrol 20, 2328–2337. [PubMed: 19729440]

Tanimura S, Ohtsuka S, Mitsui K, Shirouzu K, Yoshimura A, Ohtsubo M, 1999 MDM2 interacts with MDMX through their RING finger domains. FEBS Lett 447, 5–9. [PubMed: 10218570]

Tateossian H, Morse S, Simon MM, Dean CH, Brown SD, 2015 Interactions between the otitis media gene, Fbxo11, and p53 in the mouse embryonic lung. Dis Model Mech 8, 1531–1542. [PubMed: 26471094]

Terzian T, Wang Y, Van Pelt CS, Box NF, Travis EL, Lozano G, 2007 Haploinsufficiency of Mdm2 and Mdm4 in tumorigenesis and development. Mol Cell Biol 27, 5479–5485. [PubMed: 17526734]

Tollini LA, Jin A, Park J, Zhang Y, 2014 Regulation of p53 by Mdm2 E3 ligase function is dispensable in embryogenesis and development, but essential in response to DNA damage. Cancer Cell 26, 235–247. [PubMed: 25117711]

Tyner SD, Venkatachalam S, Choi J, Jones S, Ghebranious N, Igelmann H, Lu X, Soron G, Cooper B, Brayton C, Park SH, Thompson T, Karsenty G, Bradley A, Donehower LA, 2002 p53 mutant mice that display early ageing-associated phenotypes. Nature 415, 45–53. [PubMed: 11780111]

Valentin-Vega YA, Box N, Terzian T, Lozano G, 2009 Mdm4 loss in the intestinal epithelium leads to compartmentalized cell death but no tissue abnormalities. Differentiation 77, 442–449. [PubMed: 19371999]

Van Nostrand JL, Bowen ME, Vogel H, Barna M, Attardi LD, 2017 The p53 family members have distinct roles during mammalian embryonic development. Cell Death Differ 24, 575–579. [PubMed: 28211873]

Van Nostrand JL, Brady CA, Jung H, Fuentes DR, Kozak MM, Johnson TM, Lin CY, Lin CJ, Swiderski DL, Vogel H, Bernstein JA, Attie-Bitach T, Chang CP, Wysocka J, Martin DM, Attardi LD, 2014 Inappropriate p53 activation during development induces features of CHARGE syndrome. Nature 514, 228–232. [PubMed: 25119037]

Vousden KH, 2002 Activation of the p53 tumor suppressor protein. Biochim Biophys Acta 1602, 47–59. [PubMed: 11960694]

Vousden KH, Lane DP, 2007 p53 in health and disease. Nat Rev Mol Cell Biol 8, 275–283. [PubMed: 17380161]

Wu X, Bayle JH, Olson D, Levine AJ, 1993 The p53-mdm-2 autoregulatory feedback loop. Genes Dev 7, 1126–1132. [PubMed: 8319905]

Xiong S, Van Pelt CS, Elizondo-Fraire AC, Liu G, Lozano G, 2006 Synergistic roles of Mdm2 and Mdm4 for p53 inhibition in central nervous system development. Proc Natl Acad Sci U S A 103, 3226–3231. [PubMed: 16492743]

Zhang Y, Zeng SX, Hao Q, Lu H, 2017 Monitoring p53 by MDM2 and MDMX is required for endocrine pancreas development and function in a spatio-temporal manner. Dev Biol 423, 34–45. [PubMed: 28118981]

Zhang Y, Zhang X, Lu H, 2014 Aberrant activation of p53 due to loss of MDM2 or MDMX causes early lens dysmorphogenesis. Dev Biol 396, 19–30. [PubMed: 25263199]

Zhao H, Kegg H, Grady S, Truong HT, Robinson ML, Baum M, Bates CM, 2004 Role of fibroblast growth factor receptors 1 and 2 in the ureteric bud. Dev Biol 276, 403–415. [PubMed: 15581874]

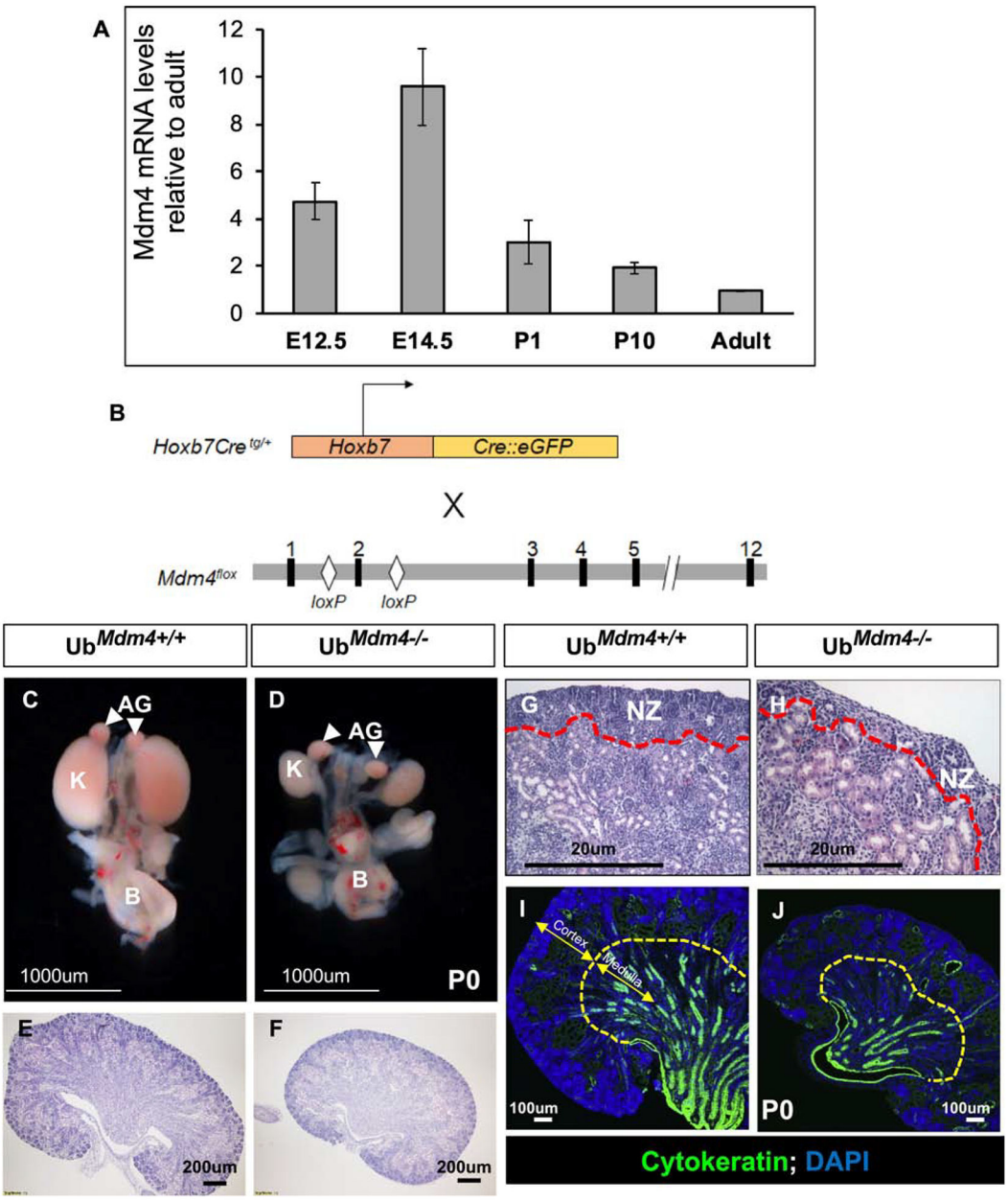

Figure 1. Deletion of *Mdm4* from the Ub lineage impairs kidney growth.

(A) Developmental expression of *Mdm4* in mouse kidneys assessed by qRT-PCR. (B) Strategy for targeted *Mdm4* deletion in Ub lineage. (C, D) Gross view of the urogenital tract showing small kidneys in newborn Ub$^{Mdm4-/-}$ compared to control Ub$^{Mdm4+/+}$ mice. H&E staining of kidney sections showing small overall size (E, F) and thinner nephrogenic zone (G, H) in Ub$^{Mdm4-/-}$ mice. (I, J) Newborn Ub$^{Mdm4-/-}$ mice revealed poor medullary development of kidneys by section immunofluorescence staining.

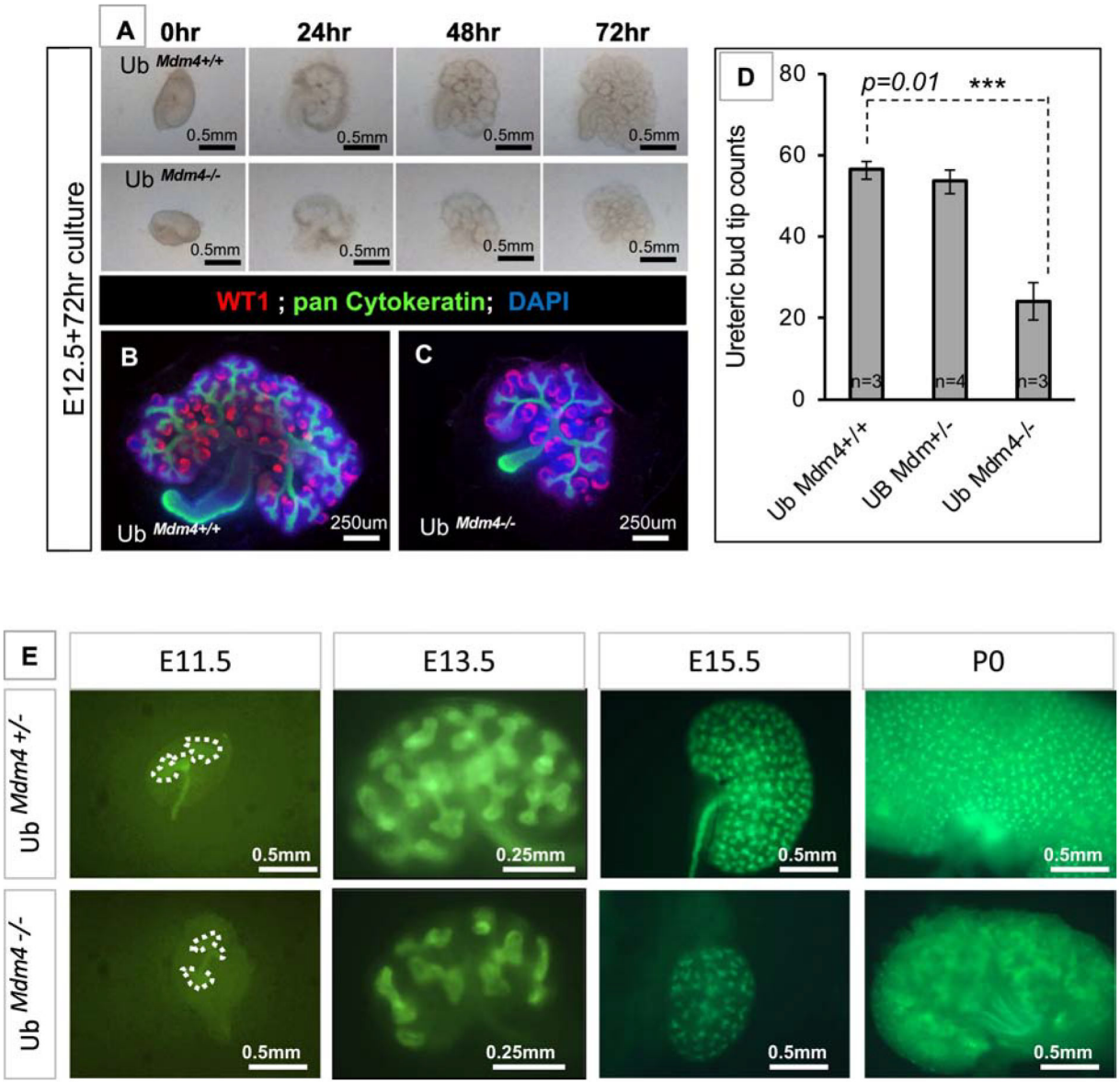

Figure 2. Embryonic Ub$^{Mdm4-/-}$ kidneys have impaired branching morphogenesis.

Whole mount phase contrast microscopy (A) and immunofluorescence staining (B–C) of E12.5 metanephric explants cultured for 72 hrs. (D) Bar graph showing Ub tip counts across the different genotypes. (E) GFP immunofluorescence of E11.5, E13.5, E15.5 and P0 metanephroi.

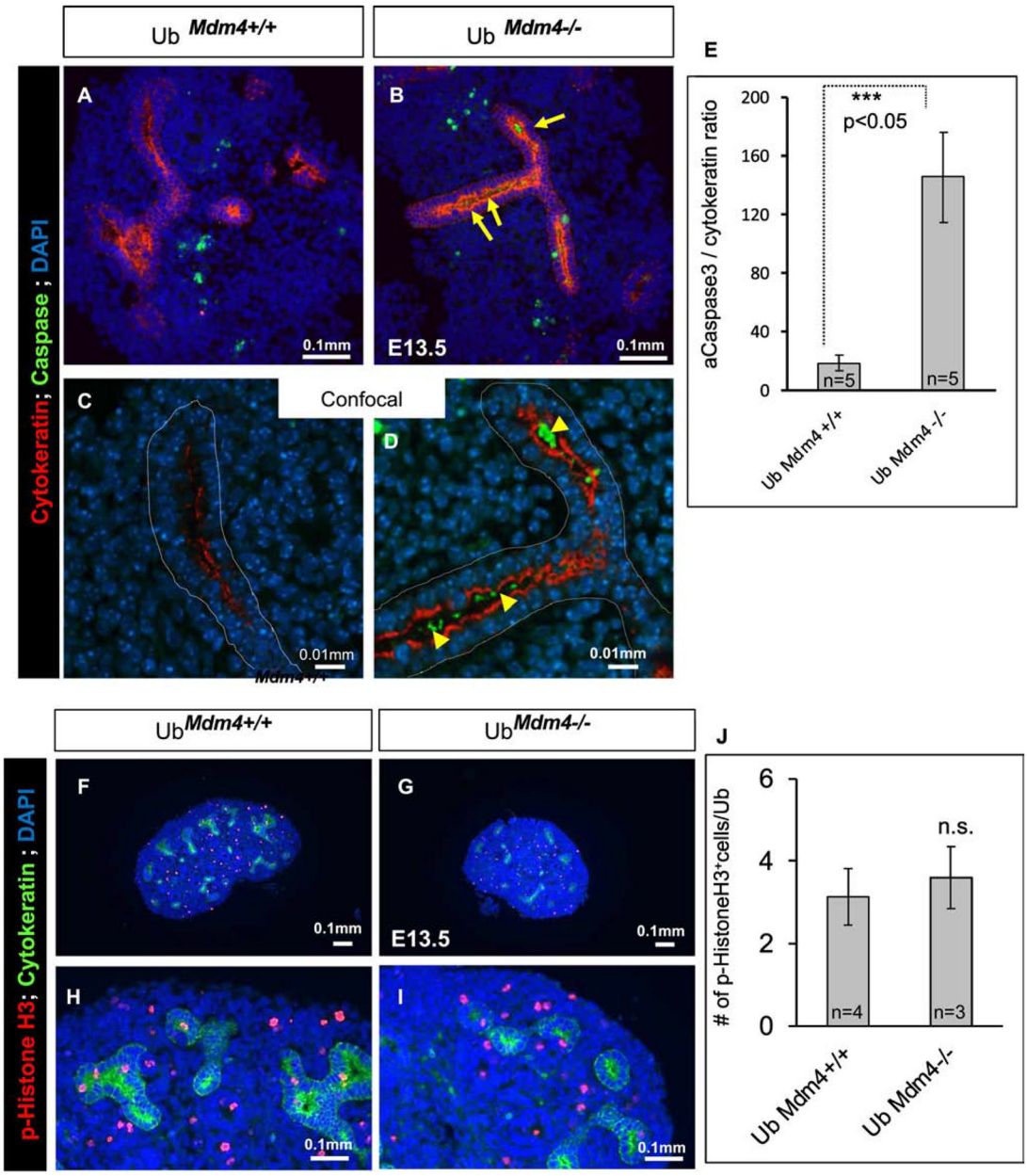

Figure 3. Increased apoptosis in E13.5 Ub$^{Mdm4-/-}$ kidneys.

(A–D) Ub$^{Mdm4+/+}$ kidneys have foci of apoptotsis (aCaspase-3 positive foci) in the mesenchyme, whereas Ub$^{Mdm4-/-}$ kidneys show apoptotic cells lining Ub branches (arrows) and in their lumen (arrowheads). (E) Quantitative analysis of Ub cell apoptosis. Each column represents an n of 5. The error bars represent S.E.M values. (F–J) Spatial distribution and quantitation of proliferating cells in Ub branches is similar in Ub$^{Mdm4+/+}$ and Ub$^{Mdm4-/-}$ kidneys. Abbreviation: ns, not significant

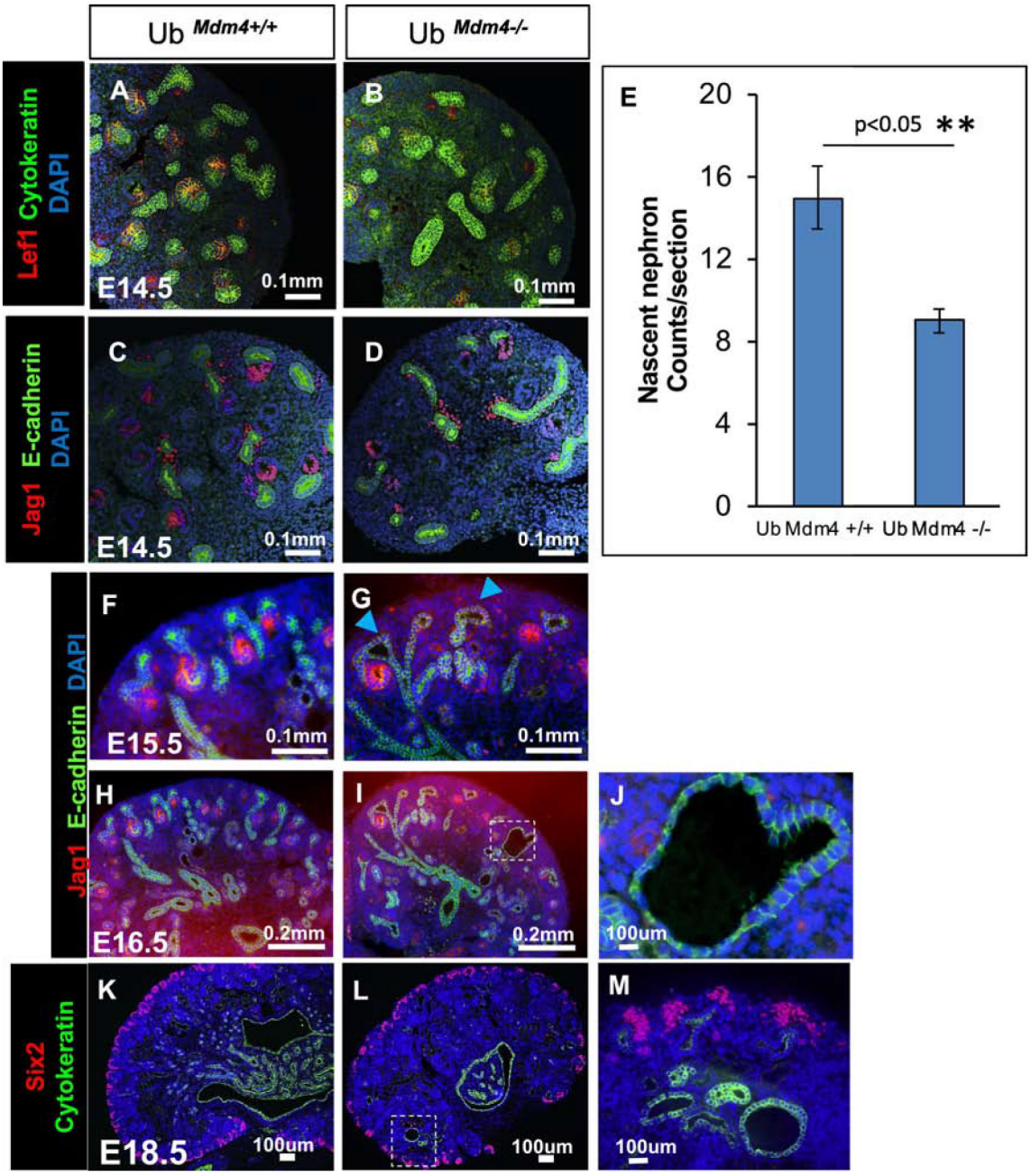

Figure 4. Impaired nephron formation in embryonic Ub$^{Mdm4-/-}$ kidneys.

Section immunofluorescence staining of Lef1 (A,B) and Jagged1 (C,D) showing reduced number of nascent nephrons in Ub$^{Mdm4-/-}$ as compared to Ub$^{Mdm4+/+}$ kidneys. (E) quantitation of nascent nephron number. (F-M) Abnormally dilated Ub ampullae and collecting ducts (arrowheads in G; squares in I,J,L,M) in Ub$^{Mdm4-/-}$ kidneys.

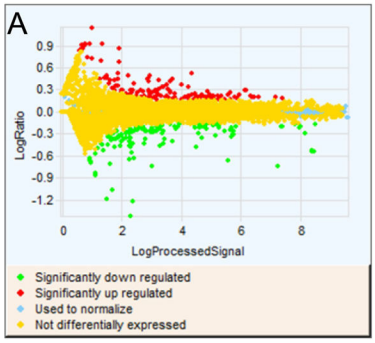

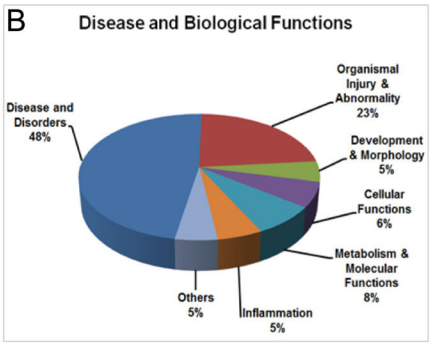

C

Top Analysis-Ready Molecules

Expression fold change up-regulated

Molecules	Expr.value
Eif2s3y	18.257
DDX3Y	12.203
CDKN1A	10.449
PLCD4	10.028
KDM5D	8.737
Uty	7.803
ZNF226	7.651
S100A8	4.842
GDF15	4.677
S100A9	4.627

Expr Fold Change down-regulated

Molecules	Expr. Value
ZFP30	-4.278
GSDMC	-3.339
ZFP82	-2.916
1700086L19Rik	-2.847
PPIL4	-2.719
SLC16A5	-2.716
PIANP	-2.691
KRT36	-2.557
ZNF569	-2.469
CR2	-2.434

D

Ub-enriched genes

Gene symbol	Expr Fold Change	Location
SOX8	-2.074	Nucleus
CRLF1	-1.795	Extracellular Space
CALB1	-1.608	Cytoplasm
RPRM	-1.603	Cytoplasm
SLCO4C1	-1.581	Plasma Membrane
TMEM59L	-1.509	Cytoplasm
ETV4	-1.496	Nucleus
GFRA1	-1.491	Plasma Membrane
DOK6	-1.454	Cytoplasm
WNT11	-1.351	Extracellular Space
CPA2	-1.336	Extracellular Space
GJA1	-1.325	Plasma Membrane
FN1	-1.306	Extracellular Space
AXIN2	-1.299	Cytoplasm
C11orf54	-1.297	Nucleus
ROS1	-1.274	Plasma Membrane
CTNND2	-1.25	Plasma Membrane
UHRF1	-1.236	Nucleus
KDM2B	-1.219	Nucleus
C18orf54	-1.215	Extracellular Space
MOXD1	-1.214	Cytoplasm
LHX1	-1.21	Nucleus
TMPO	1.211	Nucleus
PSRC1	1.245	Cytoplasm
ADAMTS18	1.294	Extracellular Space
AK1	1.321	Cytoplasm
SERPINE2	1.333	Extracellular Space
SOCS2	1.431	Cytoplasm

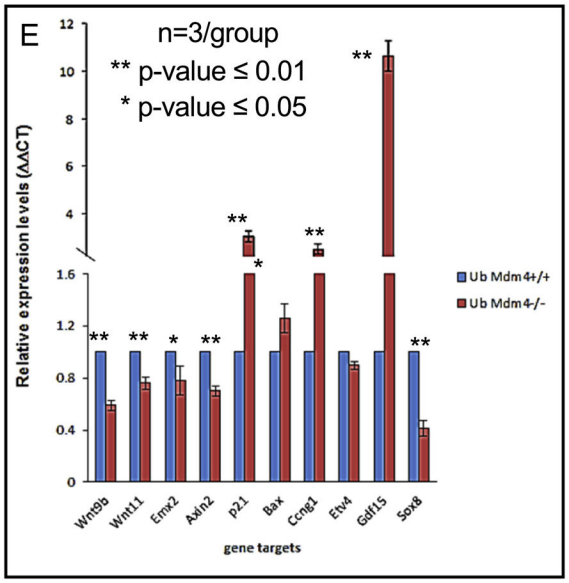

Figure 5. Microarray-based transcriptional profiling of E14.5 Ub$^{Mdm4+/+}$ and Ub$^{Mdm4-/-}$ kidneys (n=4/group).

(A) Significantly up- and down-regulated genes. (B) IPA aided analysis of disease biological functions affected in Ub$^{Mdm4-/-}$ kidneys. (C) IPA aided top analysis of most upregulated and downregulated genes in Ub$^{Mdm4-/-}$ kidneys. (D) Most significantly upregulated and downregulated genes that are highly enriched in Ub (Rutledge et al, 2017). (E) Quantitative RT-PCR of gene expression to validate expression of selected differentially expressed genes.

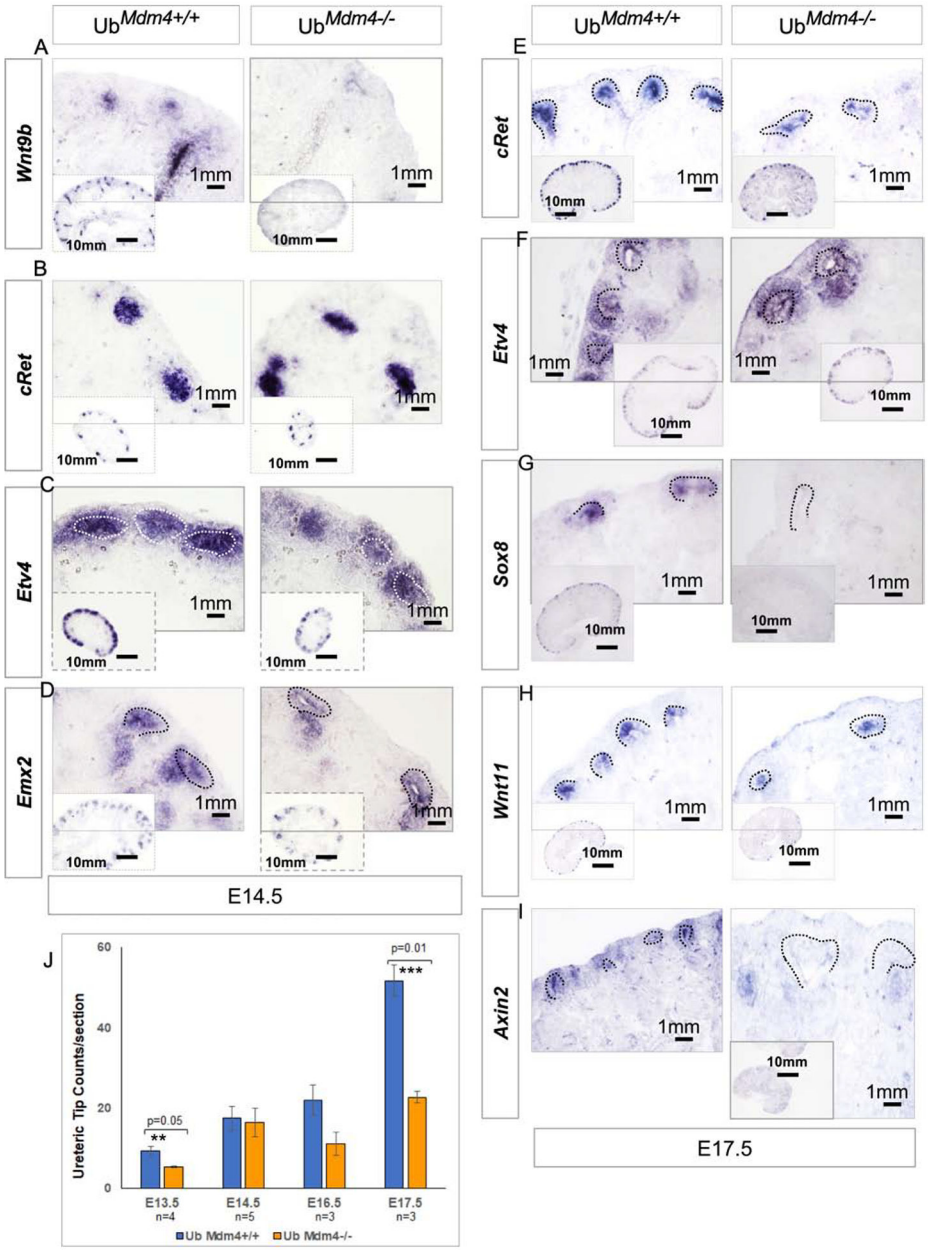

Figure 6. Ub marker expression in Ub$^{Mdm4+/+}$ and Ub$^{Mdm4-/-}$ kidneys.

Section hybridization at E14.5 (A–D) and E17.5 (E–I). (J) Quantitation of UB tips in various age groups.

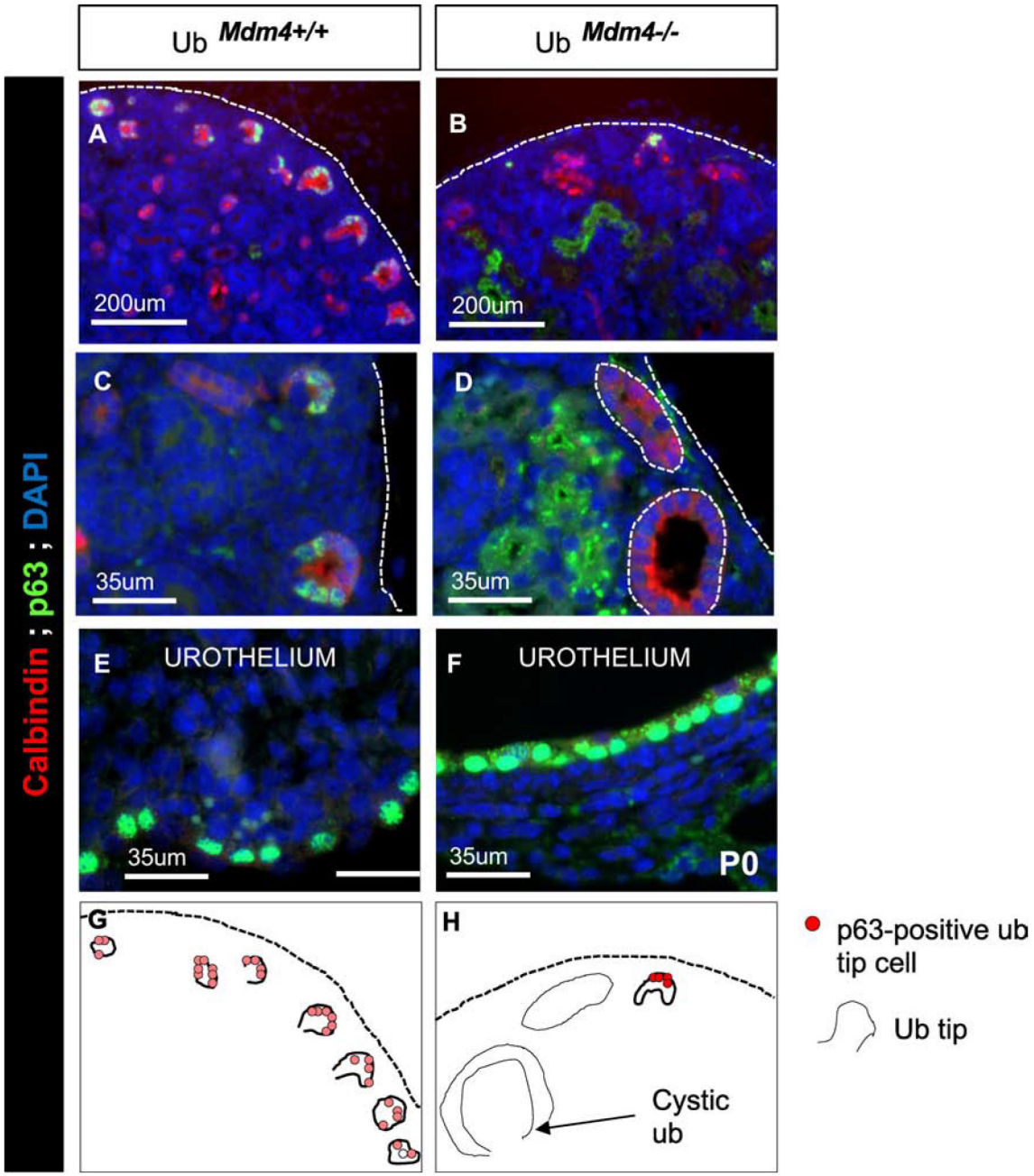

Figure 7. Loss of p63-positive Ub tip expressing cells in Ub$^{Mdm4-/-}$ kidneys.

P63, a member of the p53 gene family, labels Ub tip cells after E15.5 in wild-type kidneys (A, C). Expression of p63 appear strong in the few persisting tips in Ub$^{Mdm4-/-}$ kidneys (B, D) and is preserved in the urothelium (E, F). (G, H) Schematic of p63 expression in Ub tips.

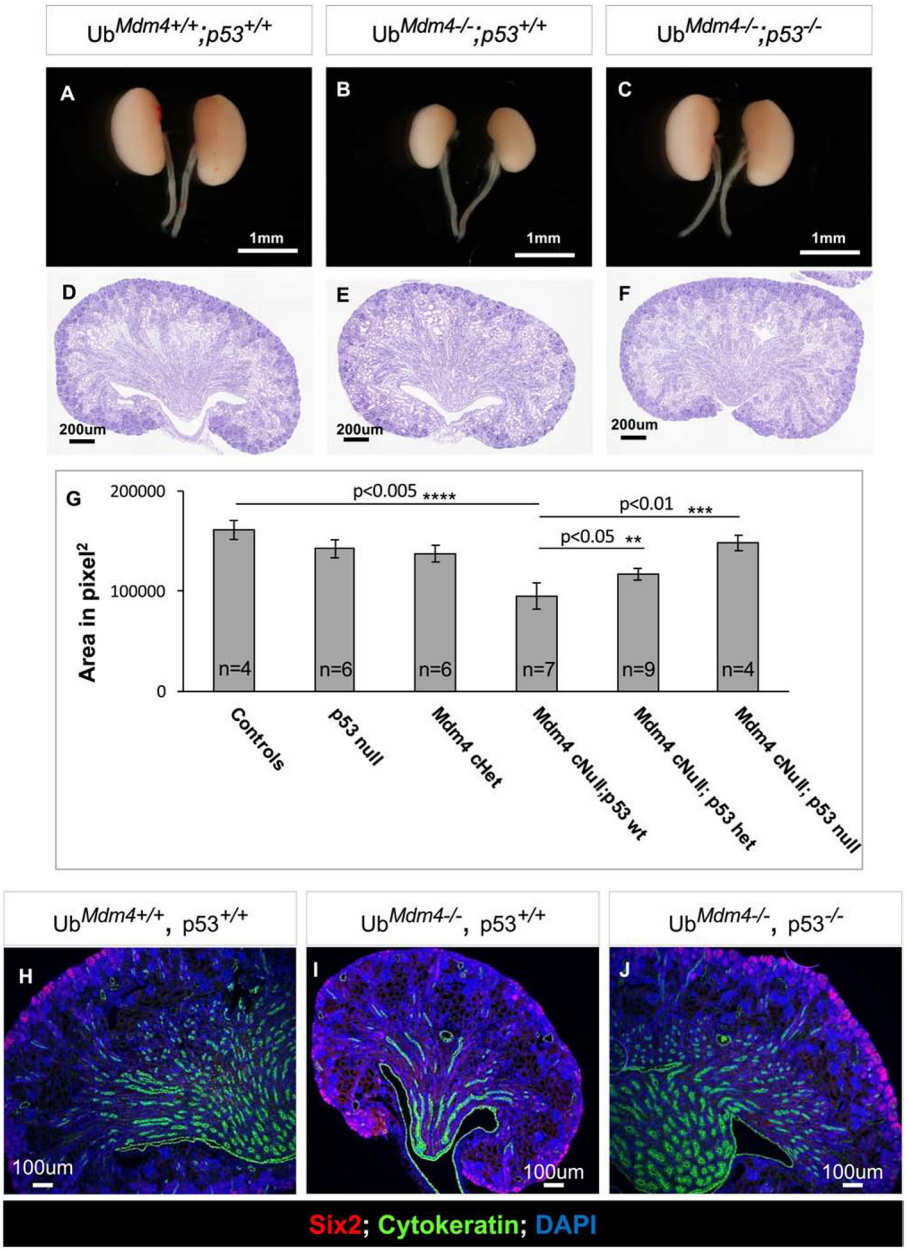

Figure 8. Deletion of *p53* rescues the renal phenotype of Ub$^{Mdm4-/-}$ kidneys.

(A–C) Gross morphology and (D–F) H&E-stained sections showing restoration of kidney size and the nephrogenic zone and medulla in Ub$^{Mdm4-/-}$; p53$^{-/-}$ kidneys. (G) Quantitative analysis of kidney surface area showing restoration of kidney size in Ub$^{Mdm4-/-}$; p53$^{-/-}$ kidneys. (H–J) Section immunofluorescence showing restoration of Six2^{+} nephron progenitors and cytokeratin^{+} collecting ducts in Ub$^{Mdm4-/-}$; p53$^{-/-}$ kidneys.

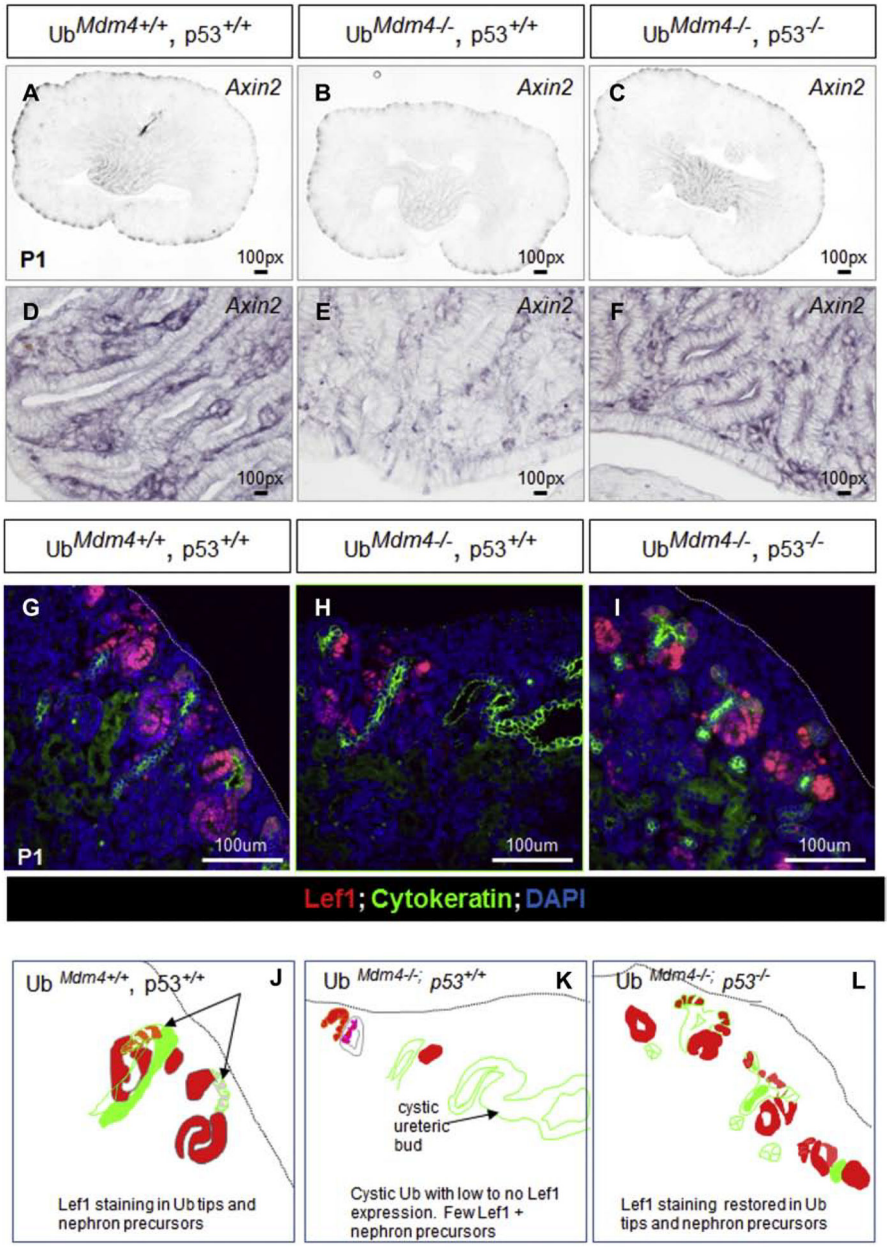

Figure 9. Restored Wnt signaling in Ub$^{Mdm4-/-}$; p53$^{-/-}$ kidneys.

(A–F) In situ hybridization showing restoration of *Axin2* expression in the renal medulla of Ub$^{Mdm4-/-}$; p53$^{-/-}$ kidneys. (G–I) Restored expression of Lef1 in Ub and nascent nephrons of Ub$^{Mdm4-/-}$; p53$^{-/-}$ kidneys. (J–L) Schematic representation of the findings in G–I.

Table1:

Genes altered in both the Ub$^{Mdm4-/-}$ and the *Wnt9b*$^{-/-}$ datasets

Gene Name	Gene Symbol	Agilent	Expr FC	Location	Type(s)
glial cell derived neurotrophic factor	Gdnf	A_55_P2745662	−1.65	Extracellular Space	growth factor
cadherin 4	Cdh4	A_52_P181943	−1.36	Plasma Membrane	other
C-X-C motif chemokine receptor 4	Cxcr4	A_55_P2745744	−1.294	Plasma Membrane	G-protein coupled receptor
Wnt family member 4	Wnt4	A_66_P139703	−1.24	Extracellular Space	cytokine
paired box 8	Pax8	A_66_P118214	−1.236	Nucleus	transcription regulator
lymphoid enhancer binding factor 1	Lef1	A_55_P2076871	−1.208	Nucleus	transcription regulator
integrin subunit alpha 8	Itga8	A_51_P309920	1.227	Plasma Membrane	other
glutathione peroxidase 6	Gpx6	A_51_P299149	1.279	Extracellular Space	enzyme

Table 2:

p53 gene targets altered in the *Hoxb7Cre-Mdm4* array.

Symbol	Entrez Gene Name	Expr Fold Change
CDKN1A	cyclin dependent kinase inhibitor 1A	10.449
PERP	PERP, TP53 apoptosis effector	3.473
CCNG1	cyclin G1	2.132
FAS	Fas cell surface death receptor	1.696
TP53INP1	tumor protein p53 inducible nuclear protein 1	1.629
APAF1	apoptotic peptidase activating factor 1	1.347
PIK3R4	phosphoinositide-3-kinase regulatory subunit 4	1.333
SERPINE2	serpin family E member 2	1.333
ADGRB1	adhesion G protein-coupled receptor B1	1.283
SNAI2	snail family transcriptional repressor 2	1.278
THBS1	thrombospondin 1	1.209
TOPBP1	topoisomerase (DNA) II binding protein 1	−1.201
FGFR2	fibroblast growth factor receptor 2	−1.207
PIK3C2A	phosphatidylinositol-4-phosphate 3-kinase catalytic subunit type 2 alpha	−1.219
CTNNB1	catenin beta 1	−1.276
AKT2	AKT serine/threonine kinase 2	−1.303
MAPK8	mitogen-activated protein kinase 8	−1.35
AKT1	AKT serine/threonine kinase 1	−1.391
PIK3R2	phosphoinositide-3-kinase regulatory subunit 2	−1.451
RPRM	reprimo, TP53 dependent G2 arrest mediator homolog	−1.603

Table 3:

A list of select genes common to Mdm4-Hoxb7Cre array and embryonic kidney p53 Chip Seq (Physiol Genomics 45, 948–964).

		p53 chip seq E15.5	Mdm4flox-Hox7Cre E14.5		
Symbol	**Entrez Gene Name**	**Fold affinity**	**Expr Fold Change**	**Location**	**Type(s)**
CDKN1A	cyclin dependent kinase inhibitor 1A	16	10.449	Nucleus	kinase
EDA2R	ectodysplasin A2 receptor	18	3.651	Plasma Membrane	transmembrane receptor
SP6	Sp6 transcription factor	20	1.832	Nucleus	transcription regulator
KLF13	Kruppel like factor 13	13	1.617	Nucleus	transcription regulator
ITGB4	integrin subunit beta 4	17	1.514	Plasma Membrane	transmembrane receptor
GPR65	G protein-coupled receptor 65	15	1.427	Plasma Membrane	G-protein coupled receptor
KLF4	Kruppel like factor 4	10	1.409	Nucleus	transcription regulator
SLIT2	slit guidance ligand 2	19	1.36	Extracellular Space	other
MMP19	matrix metallopeptidase 19	25	1.329	Extracellular Space	peptidase
CDH6	cadherin 6	20	1.324	Plasma Membrane	other
PCDH8	protocadherin 8	23	1.296	Plasma Membrane	other
TEAD1	TEA domain transcription factor 1	23	1.212	Nucleus	transcription regulator
LHX1	LIM homeobox 1	21	−1.21	Nucleus	transcription regulator
TCF4	transcription factor 4	19	−1.234	Nucleus	transcription regulator
LGR4	leucine rich repeat containing G protein-coupled receptor 4	15	−1.258	Plasma Membrane	transmembrane receptor
CTNNB1	catenin beta 1	29	−1.276	Nucleus	transcription regulator
AXIN2	axin 2	15	−1.299	Cytoplasm	other
GJA1	gap junction protein alpha 1	17	−1.325	Plasma Membrane	transporter
KLF5	Kruppel like factor 5	24	−1.327	Nucleus	transcription regulator
MAPK8	mitogen-activated protein kinase 8	19	−1.35	Cytoplasm	kinase
WNT11	Wnt family member 11	18	−1.351	Extracellular Space	other
CHD7	chromodomain helicase DNA binding protein 7	15	−1.372	Nucleus	enzyme
AKT1	AKT serine/threonine kinase 1	39	−1.391	Cytoplasm	kinase
ATP2B2	ATPase plasma membrane Ca2+ transporting 2	15	−1.425	Plasma Membrane	transporter
RNASEH2A	ribonuclease H2 subunit A	27	−1.472	Nucleus	enzyme
GADD45GIP1	GADD45G interacting protein 1	12	−1.481	Nucleus	other
ETV4	ETS variant 4	13	−1.496	Nucleus	transcription regulator
PTCH1	patched 1	25	−1.584	Plasma Membrane	transmembrane receptor
CALB1	calbindin 1	11	−1.608	Cytoplasm	other
PDE5A	phosphodiesterase 5A	12	−1.7	Cytoplasm	enzyme

		p53 chip seq E15.5	Mdm4flox-Hox7Cre E14.5		
Symbol	**Entrez Gene Name**	**Fold affinity**	**Expr Fold Change**	**Location**	**Type(s)**
RUNX2	runt related transcription factor 2	23	−1.742	Nucleus	transcription regulator
CRLF1	cytokine receptor like factor 1	20	−1.795	Extracellular Space	other